Hindawi
International Journal of Photoenergy
Volume 2019, Article ID 7945683, 14 pages
https://doi.org/10.1155/2019/7945683

Research Article

Determination of Technological Features of a Solar Photovoltaic Cell Made of Monocrystalline Silicon P^+PNN^+

Cristian-Petre Fluieraru,[1] **Gabriel Predușcă**,[1] **Horia Andrei**,[1] **Emil Diaconu**,[1] **Petru Adrian Cotfas**,[2] **and Daniel Tudor Cotfas**[2]

[1]*Department of Electronics, Telecommunications, and Energy Engineering, University Valahia of Târgoviște, Str. Aleea Sinaia, Nr. 13, RO-130004 Târgoviște, Romania*
[2]*Department of Electronics and Computer, University Transilvania of Brasov, Str. Universitatii, Nr. 1, Brasov, Romania*

Correspondence should be addressed to Cristian-Petre Fluieraru; cristi2006tgv@yahoo.com

Received 6 April 2019; Accepted 26 September 2019; Published 19 November 2019

Academic Editor: Leonardo Palmisano

The development in the field of semiconductor materials and electronic devices has a great impact on systems with renewable energy sources. Determination of the functional parameters of photovoltaic solar cells is essential for the subsequent usage of these semiconductor devices. Research was made on type P^+PNN^+ monocrystalline silicon wafers. Crystallographic measurements of the photovoltaic solar cell were made by means of FESEM-FIB Auriga Workstation. Initial data were selected from the study of models found in the specialized literature. The experimental results were compared to classical mathematical models. Measurements made on the photovoltaic solar cell were realised in laboratory conditions on the NI-ELVIS platform produced by National Instruments.

1. Introduction

Absorption of photons under certain conditions in a semiconductor plate creates electrical power. The principle of conversion is based on the fact that in a semiconductor the electrons removed from the nucleus can be transformed into free conducting electrons in motion. This creates a positive load and a negative carrier simultaneously.

If there is a potential difference in the semiconductor material due to a p-n junction, then this load carrier can be forced to direct to an external circuit and thus an electric power can be produced. In the case of crystalline silica, the electric charge carriers that have been obtained can only reach this potential barrier due to thermal vibrations. No other force can lead them in this direction. This means that loaded particles will have to survive until they reach the potential barrier. The resulting lifetime is one of the key factors for the efficiency of photovoltaic energy production [1].

The physical effect was first observed by Becquerel in 1839 when he obtained power by exposing silver electrodes to radiation in an electrolyte. The effect was further described by Adams and Day in 1877 [2, 3]. They noticed that the exposure of selenium electrodes to radiation produces electrical voltage thus allowing them to obtain electrical power. Until 1949, when the semiconductor appeared, the photovoltaic effect was not used. Then in 1954, in the US, Chapin developed the first solar cell based on crystalline silicon, which had a 6% efficiency (very good for those times) [4]. In the coming years, efficiency has increased to 10%.

The main reason for the spread of the application of the photovoltaic effect to energy sources was the oil crisis of 1973. Since that time, specific research institutes have emerged around the world. At the beginning of the 1980s, it was recognized that the efficiency of solar cells is very important for reducing the cost of alternative energy systems. From this point on, research and development have been focused on achieving greater efficiency. For the future, it is expected that with the disappearance of fossil fuels, the Sun will be one of the few inexhaustible sources of energy widely used.

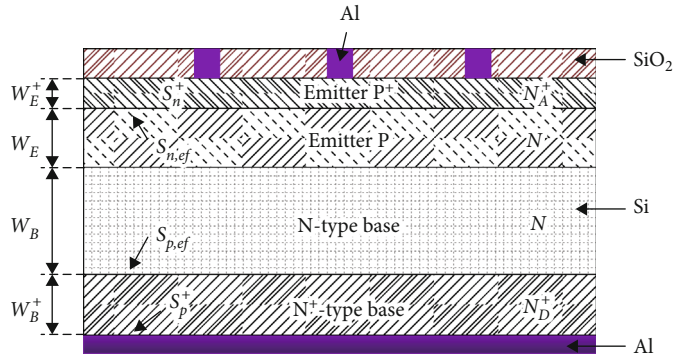

Figure 1: The structure of the analysed photovoltaic cell.

The efficiency record is 24-27% and is owned by a monocrystalline silicon solar cell using very complex technology [5, 6].

Cells currently commercially produced have an efficiency of between 14% and 16%. In particular cases, cells that stretch on larger surfaces have an efficiency of between 17% and 19% [7, 8].

In general, the efficiency of photovoltaic energy conversion is very limited of physical causes [9]. Approximately 24% of the solar radiation has a wavelength so large that it cannot be absorbed. In addition, 33% is lost as heat. The following 15-20% losses occur because the cell voltage reaches only 70% of the value corresponding to the energy range [10].

From the recent literatures, it was found that there are no studies on parasitic resistance and characteristics of PV cells made of monocrystalline silicon P^+PNN^+.

This study aims to determine the technological characteristics of PV cell monocrystalline silicon P^+PNN^+. The present work has five sections. Section 1 covers a review of the literature. Section 2 is based on the experimental setup and methodology of the studied PV cell. Determination and analysis of technological parameters of the studied PV cell are discussed in Section 3. Afterwards, the experimental results are interpreted in Section 4 and compared to theoretical ones. Section 4 provides concluding remarks.

2. Experimental Setup and Methodology

Monocrystalline silicon solar photovoltaic cells are the most stable from the family of photovoltaic cells made of silicon [10–15].

The processing of monocrystalline silicon for obtaining semiconductor devices for solar photovoltaic cells is a complex manufacturing process [16–18]. The studied cells are manufactured at ICPE-Bucharest, and they are type P^+PNN^+ solar photovoltaic cells (see Figures 1 and 2). There were type p silicon wafers used for its manufacturing. The production flow chart contains a couple of basic stages, each of it containing a few specific operations with longer or shorter processing times for semiconductor structures, such as photolithography and multiple high-temperature chemical processes. The attributes of semiconductor silicon devices are strongly influenced by temperature [19].

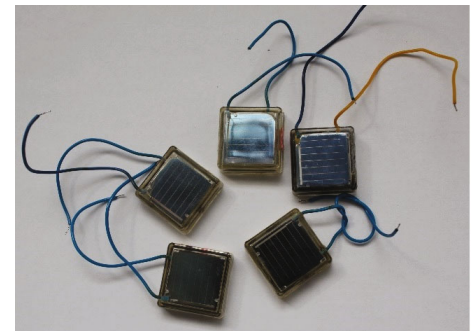

Figure 2: Photovoltaic cell type P^+PNN^+.

Semiconductor junctions lay at the foundation of manufacturing and functioning of the majority of semiconductor device categories. Related to conversion efficiency and power output, it is considered that the best results are obtained for the photovoltaic solar cells with p-n junctions [20]. Hence, if two semiconductor materials such as type p and type n are put in contact, they create the p-n junction of the material. Practically, this represents the separation area between the two regions [21], the type p semiconductor being doped with acceptor atoms (for instance, boron) and the type n semiconductor being doped with donor atoms (for instance, phosphorus). Pursuant to the diffusion of majority carriers in the junction area, there appears an area of positive spatial charge in layer n and an area of negative charge in layer p. In this situation, the electric field oriented from layer n to layer p appears [20, 22–24].

Crystallographic measurements of the photovoltaic solar cell were made by means of Auriga FESEM-FIB Workstation equipment. In Figure 3, the SEM analysis in a longitudinal section on a metallic face at a resolution of 100 μm is presented.

X-ray diffraction is an analytic technique which offers structural and chemical information about the crystallography of a range of various materials [25], such as the crystallographic structure of the material, structural analysis of the material, surface analysis of the material, analysis of thin layers, and transformation due to the influence of temperature (see Figures 4 and 5) [25–27]. Graphics data processing was made by the representation of data acquired using a D8 DISCOVER diffractometer, Bruker AXS GmbH.

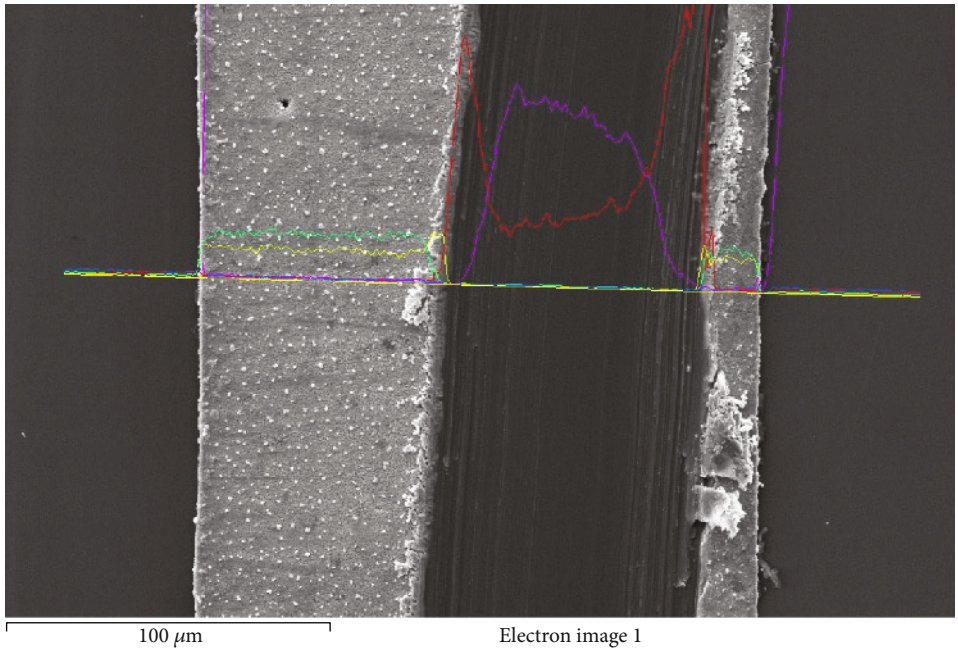

Figure 3: SEM analysis in a longitudinal section at a resolution of 100 μm.

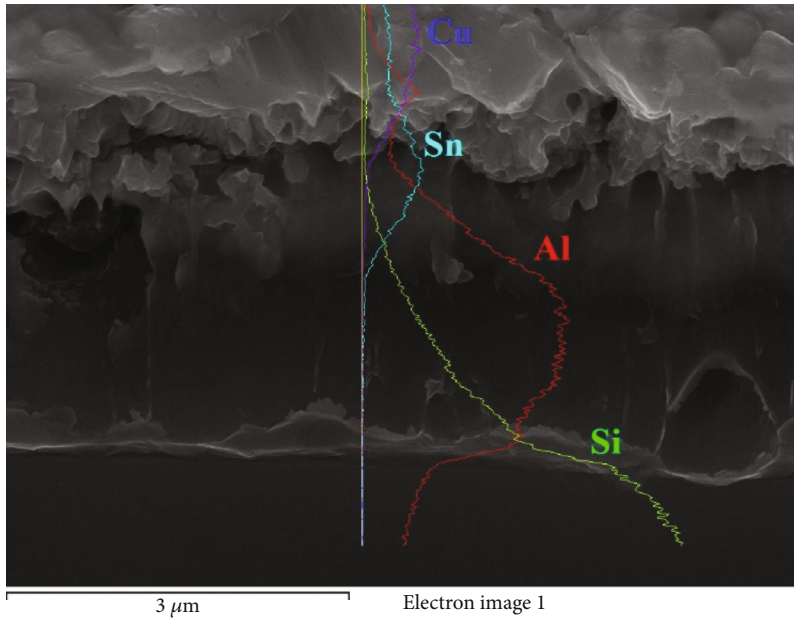

Figure 4: SEM and EDX for the upper part of the metal-faced layer of a photovoltaic solar cell.

Silicon is one of the hardest materials to interpret by X-ray diffraction. In order to be subjected to X-ray diffraction, the analysed cell was treated with hydrofluoric acid for 1-3 minutes, because above it is the SiO_2 layer, after which it was ultrasonicated in ionized water and finally dried with a flow of Azote. We identified with Si and the presence of silicon oxide. On one side of the platelet, the silicon oxide was intentionally created. On the other hand, the amount of oxide is small and is due to an accumulation of oxide time on the surface of the single crystalline platelets. From the X-ray diffraction spectra for the solar cell, we observed a shift of the peaks corresponding to the monocrystalline silicon. I noticed not only the additional peaks corresponding to the dopants but also the peaks corresponding to the metal impurities from the metal contacts.

2.1. Data Acquisition of Technological Parameters. The determination of functional parameters of photovoltaic solar cells is essential for the subsequent usage of these semiconductor devices. This is of major interest to manufacturers of such devices, because the parameter's improvement has as an effect on the growth of

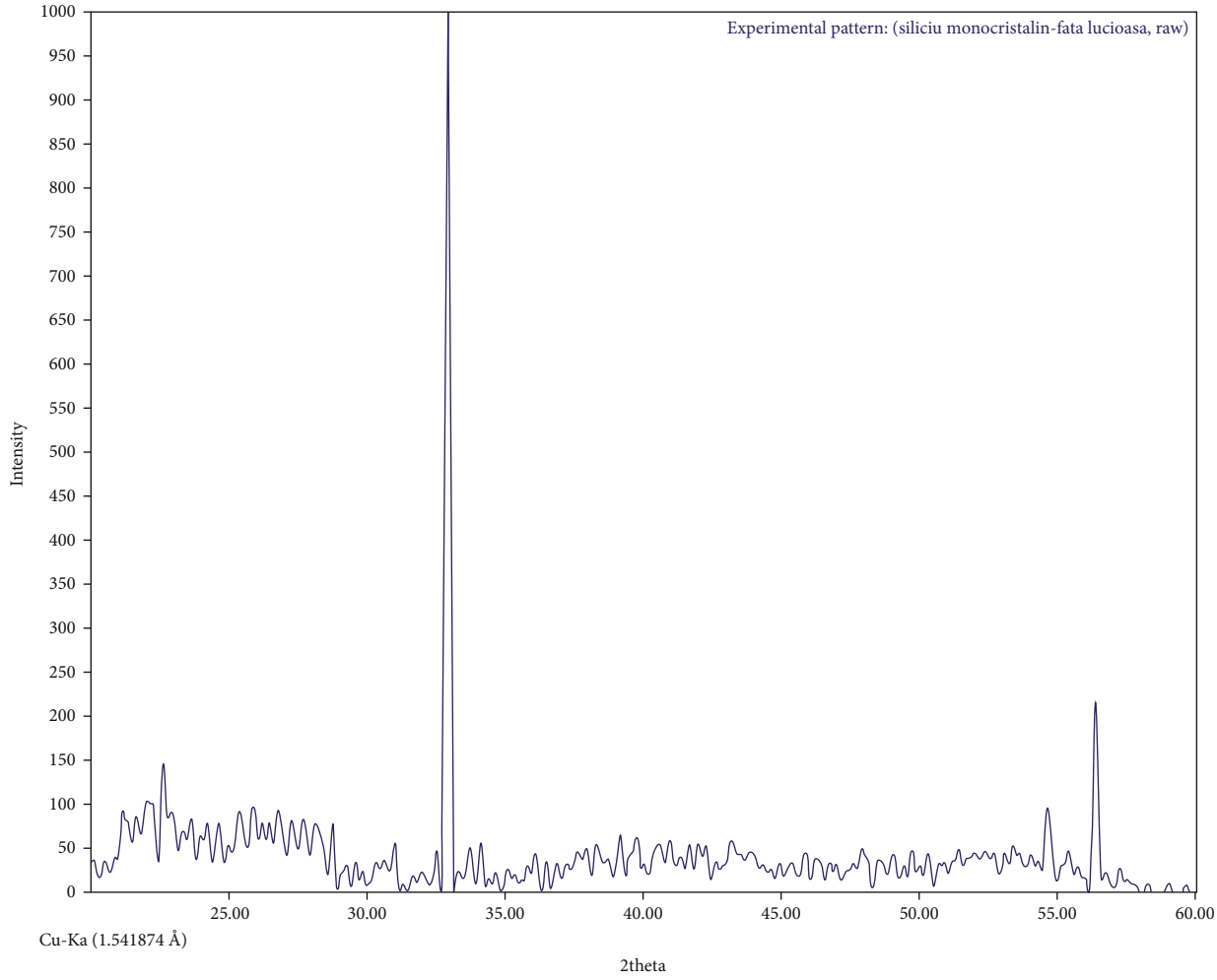

Figure 5: Diffractometry spectrum realised using X-ray on smooth-faced of monocrystalline silicon solar cell.

photovoltaic cells' efficiency [13–21]. Measurements made on the photovoltaic solar cell were realised in laboratory conditions on the NI-ELVIS platform produced by National Instruments (see Figure 6) [26, 27].

I-V characteristics were determined by monitoring the current getting through the photovoltaic solar cell at various temperatures and illumination levels. The values obtained for short-short-circuit current I_{sc} and open circuit voltage V_{oc} were determined using NI-Elvis board and LabView software (see Figure 7).

2.2. Interpretation of I-V Characteristics of the Studied Photovoltaic Solar Cell. The *I-V* characteristics of the measured solar cell were represented and after that fitted using the theoretical model with two exponentials, according to the following relation [28, 29]:

$$I = I_{01} \cdot \exp\left(\frac{V - R_s \cdot I}{(kT/q) \cdot n_1}\right) + I_{02} \cdot \exp\left(\frac{V - R_s \cdot I}{(kT/q) \cdot n_2}\right) + \frac{V}{R_p}, \quad (1)$$

where I is the solar cell current, I_{01} is the saturation current of the diffusion component, I_{02} is the saturation current of the recombination component, R_s is the parasitic series resistance, R_p is the parasitic parallel (shunt) resistance, n_1 is the ideal factor of the diffusion current, and n_2 is the ideal factor of the recombination current.

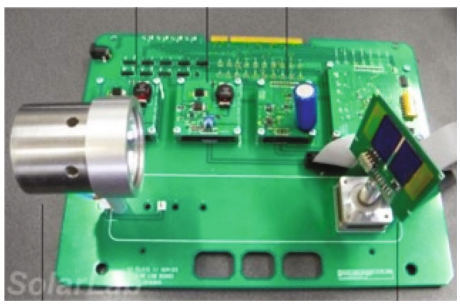

Figure 6: NI-ELVIS platform.

The current in equation (1) contains two components:

(i) A diffusion component representing the contribution of optic-generated carriers which move by diffusion

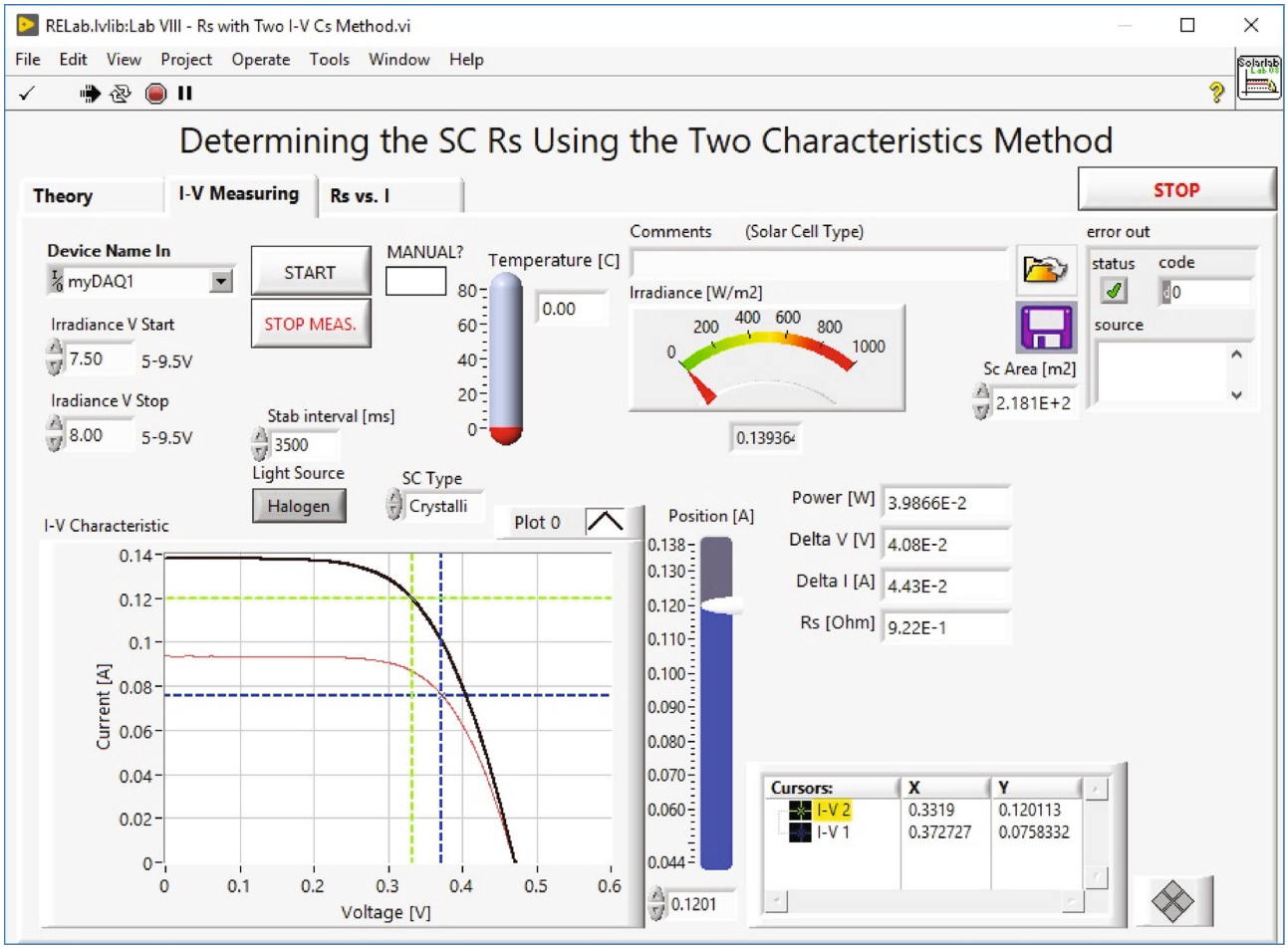

FIGURE 7: I_{sc} and V_{oc} study of the solar cell, as a function of temperature using the NI-ELVIS acquisition boards and LabView software.

in neutral regions of the p-n junction. For this component, it was considered that the ideal parameter n is the theoretical one, namely $n_1 = 1$

(ii) The second exponential component of the solar cell's current is given by the recombination of carriers in the transition region of the p-n junction. It was considered that the recombination process is mainly controlled by the Shockley-Read-Hall recombination from the respective region, being produced by the existence of the contamination of metallic impurities in that area [30, 31]. Because the most profound metallic impurities, namely the ones that have the energetic level close to the forbidden bandwidth of silicon, are the ones that determine the recombination velocities, they were used as an ideal parameter for this current component, $n_2 = 2$

The values of parasitic resistances were determined by means of an experiment, and they have the following values: $R_s = 0.750\,\Omega$ and $R_p = 379\,\Omega$.

From measurement analysis, using the equation with 2 currents, considering $n_1 = 1$, $n_2 = 2$, $R_s = 0.75\,\Omega$, and $R_p = 379\,\Omega$ and using Mathematica soft for the determination of the parameters by overlapping the curves (see Figures 8 and 9), the following values have been obtained (Table 1):

2.3. Analysis of Recombination Saturation Current I_{02}. Recombination saturation current of a photovoltaic solar cell with the p-n junction is given by the following relation:

$$I_{02} = qw\frac{n_i}{2\tau}A \tag{2}$$

where q is the electron's charge, w is the thickness of the transition region emitter base in direct polarization, n_i is the intrinsic concentration of carriers within silicon, A is the junction area emitter base, and τ is the lifetime of minority carriers from the silicon wafer volume.

The component of current I_{02} depends on the temperature by the medium of the intrinsic concentration n_i. In the range of the measured temperature $T = 32 - 37°C$, this variation is very weak and can be neglected. Abnormal values, derived from measuring errors or errors of overlapping of the curves, were deleted.

From Table 1, the medium value of recombination saturation current, characteristic of a photovoltaic solar cell, is

$$I_{02} \approx 2 \times 10^{-9}\ \text{A}. \tag{3}$$

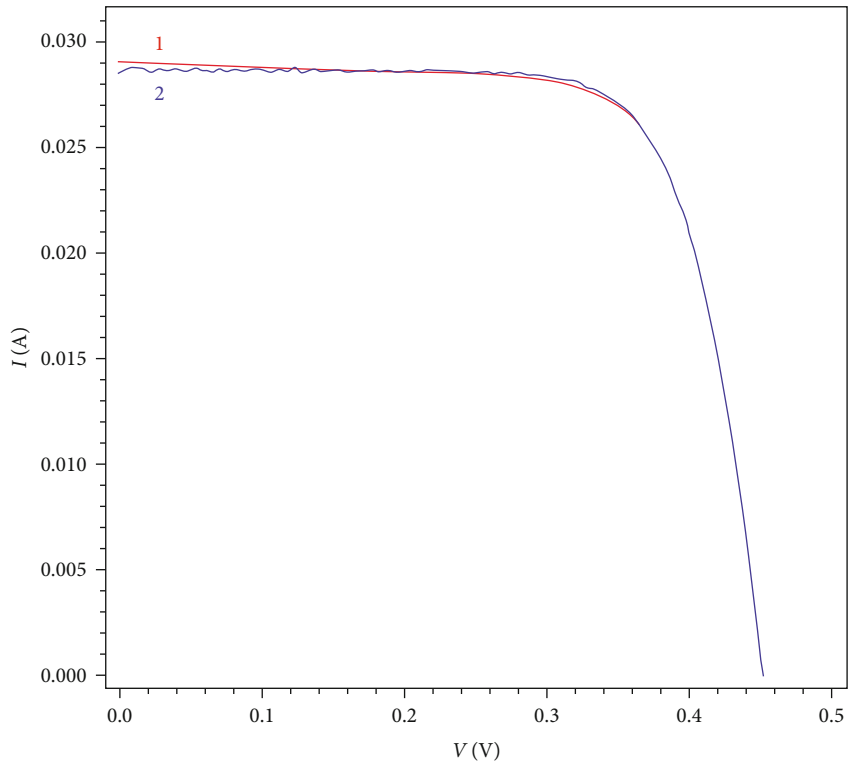

Figure 8: I-V diagram of solar cell 1 for $I_{ph} = 0.0291$ A (2) and overlapping of curves (1).

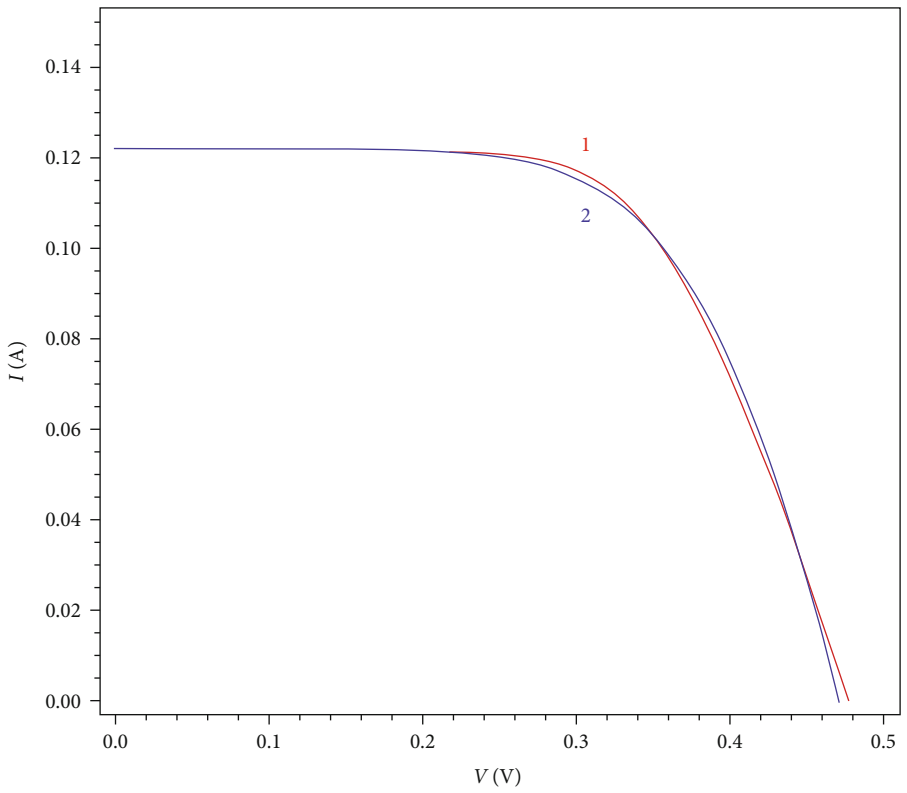

Figure 9: I-V diagram of solar cell 1 for $I_{ph} = 0.1225$ A (2) and overlapping of curves (1).

Table 1: Determination of the parameters of a photovoltaic solar cell.

I_{ph} (A)	I_{01} (A)	I_{02} (A)	T (°C)
0.0291	9.76×10^{-10}	4.37×10^{-9}	31.96
0.0357	1.38×10^{-9}	1.49×10^{-9}	32.50
0.0430	2.31×10^{-9}	2.05×10^{-9}	32.86
0.0512	2.1×10^{-9}	2.13×10^{-9}	33.17
0.0604	1.52×10^{-9}	1.58×10^{-9}	33.50
0.0705	1.71×10^{-9}	1.73×10^{-9}	33.85
0.0817	3.01×10^{-9}	3.09×10^{-9}	34.24
0.0941	1.62×10^{-9}	1.63×10^{-9}	34.64
0.1077	2.34×10^{-9}	2.35×10^{-9}	35.06
0.1225	1.98×10^{-9}	1.17×10^{-9}	35.54
0.1384	2.13×10^{-9}	1.61×10^{-9}	36.04

This value allows the estimation of a lifetime of the minority carriers within the single-crystal silicon wafers used for manufacturing of the photovoltaic solar cell.

From relation (2) we have

$$\tau_{\text{medium}} = \frac{qwn_iA}{2I_{02,\text{medium}}}. \tag{4}$$

The size of transition region w of the p-n junction is computed as follows [30, 31]:

$$w = \sqrt{\frac{2\varepsilon}{q} \cdot \frac{N_A + N_D}{N_A \cdot N_D} \cdot (V_0 - V)}, \tag{5}$$

where V_0 is the internal voltage of the junction

$$V_0 = \frac{kT}{q} \cdot \ln \frac{N_A N_D}{{n_i}^2}, \tag{6}$$

and V is the direct voltage which drops on the solar cell in conditions of a maximum power output.

From the accomplished measurements are obtained,

$$V = 0.35\,\text{V}. \tag{7}$$

For the technological case,

$$\begin{aligned} N_D &= 10^{16}\,\text{cm}^{-3}, \\ N_A &= 10^{17}\,\text{cm}^{-3}, \end{aligned} \tag{8}$$

which obtains:

$$\begin{aligned} V_0 &= 26 \times 10^{-3}\,\text{V} \times \ln \frac{10^{33}\,\text{cm}^{-6}}{10^{20}\,\text{cm}^{-6}} = 60 \times 13 \times 10^{-3}\,\text{V} = 0.78\,\text{V}, \\ w &= \sqrt{\frac{2 \times 10^{-12}\,\text{F/cm}}{1.6 \times 10^{-19}\,\text{C}} \times \frac{1}{10^{16}\,\text{cm}^{-3}} \times 0.43\,\text{V}} \\ &= 0.23 \times 10^{-4}\,\text{cm} = 0.23\,\mu\text{m}. \end{aligned} \tag{9}$$

Finally, using relation (4), the lifetime results are

$$\begin{aligned} \tau_{\text{medium}} &= \frac{1.6 \times 10^{-19}\,\text{C} \times 2.3 \times 10^{-5}\,\text{cm} \times 10^{10}\,\text{cm}^{-3} \times 4\,\text{cm}^2}{2 \times 2 \times 10^{-9}\,\text{A}} \\ &= 3.7 \times 10^{-5}\,\text{s} \cong 40\,\mu\text{s}. \end{aligned} \tag{10}$$

Because of the technological conditions of the manufacturing of photovoltaic solar cells, the following range of values is used:

$$\tau_{\text{SRH}} = 1 \div 100\,\mu\text{s}. \tag{11}$$

From the interpretation of the measurements for the I-V characteristics, a first important technological characteristic of photovoltaic solar cells is deducted, namely the value of a lifetime [17].

Hereafter, a qualitative analysis of diffusion saturation current in an ideal p-n junction were made.

For the ideal diode, I_{01} has the following form [20, 21]:

$$I_{01} = qA\left(\frac{D_p}{L_p} \cdot \frac{n_i^2}{N_D} + \frac{D_n}{L_n} \cdot \frac{n_i^2}{N_A}\right), \tag{12}$$

which becomes, in the case of abrupt junction P^+N,

$$I_{01} = qA \cdot \frac{D_p}{L_p} \cdot \frac{n_i^2}{N_D}, \tag{13}$$

or

$$I_{01} = qA \cdot \sqrt{\frac{D_p}{\tau_p}} \cdot \frac{n_i^2}{N_D}, \tag{14}$$

where L_p and D_p are the length of diffusion and the diffusion coefficient of minority holes from base n doped with a concentrationN_D of donor atoms.

By contrast with the recombination component I_{02}, the diffusion current I_{01} has a variation depending on the temperature which cannot be neglected anymore. It comes from the dependence of temperature of the following terms:

$$D = \frac{kT}{q} \cdot \mu \approx T^1, \tag{15}$$

Table 2: Values obtained for a photovoltaic solar cell measured in condition AM 1.5.

I_{sc} (A)	V_{oc} (V)	T (°C)	I_{01} (A)
0.122	0.48	35.5	2×10^{-9}

$$\tau = \frac{1}{c \cdot N_T} = \frac{1}{\sigma \cdot V \cdot N_T} \approx \frac{1}{V} \approx \frac{1}{T^{1/2}}, \tag{16}$$

$$n_i \approx T^{3/2} \cdot \exp\left(-\frac{E_G}{2kT}\right). \tag{17}$$

By solving equations (15), (16), and (17) then from (14), results

$$I_{01} \approx T^{1/2} \cdot T^{1/4} \cdot T^3 \cdot \exp\left(-\frac{E_G}{kT}\right), \tag{18}$$

where $qA \approx T^{1/2}$ and $(D_p/\tau_p) = T^{1/4}$. With a good approximation, the following can be written:

$$I_{01} \approx T^4 \cdot \exp\left(-\frac{E_G}{kT}\right). \tag{19}$$

From where

$$\frac{I_{01}(T_1)}{I_{02}(T_2)} = \left(\frac{T_1}{T_2}\right)^4 \cdot \exp\left[\frac{E_G}{k} \cdot \left(\frac{1}{T_2} - \frac{1}{T_1}\right)\right]. \tag{20}$$

The experimental values obtained for a light source that approach the condition AM 1.5 are presented in Table 2.

From this table, we have

$$\begin{aligned} I_{01} &= 2 \times 10^{-9}\ \text{A}, \\ la\ T &= 309\ \text{K}. \end{aligned} \tag{21}$$

Below formula (21), the value of the diffusion component at room temperature ($T = 300$ K) was deduced. The following was obtained:

$$\begin{aligned} I_{01}(300\ \text{K}) = I_{01}(309\ \text{K}) &\cdot \left(\frac{300}{309}\right)^4 \\ &\cdot \exp\left[\frac{1.1 \times 10^3}{26} \cdot \left(\frac{300}{309} - 1\right)\right]. \end{aligned} \tag{22}$$

Then the numerical value is ((22)), we have

$$I_{01}(300\ \text{K}) = 5 \times 10^{-10}\ \text{A}. \tag{23}$$

This value will represent the main checkout key of computer models.

3. Computing Programs for Correlation of Experimental Data with Theoretical Models Using Matlab Simulations

In order to compare the obtained experimental results, the theoretical model of direct current-voltage characteristic was used when $\tau_{\text{SRH}} = 5\,\mu$s. To analyse in Matlab, we used the following material's features, constants, and calculus formulas, which are available for $T = 300$ K [17, 31]:

(i) Intrinsic carrier concentration: $n_i = 10^{10}\ \text{cm}^{-3}$

(ii) Dielectric constant: $\varepsilon = 10^{-12}$ F/cm

(iii) Electron charge: $q = 1.6 \bullet 10^{-19}$ C

(iv) Thermal potential and thermal energy: $T/q = 25.9$ mV and $kT/q = 25.9$ mV

(v) Coefficient of diffusion for load carriers:

$$D = \frac{D_0}{1 + (N/N_0)^d} D_1, \tag{24}$$

where electrons are $D_{0n} = 35\ \text{cm}^2/\text{s}$, $D_{1n} = 1.8\ \text{cm}^2/\text{s}$, $N_0 = 10^{17}\ \text{cm}^{-3}$, $d = 0.6$ and the holes are $D_{0p} = 12.5\ \text{cm}^2/\text{s}$, $D_{1p} = 1\ \text{cm}^2/\text{s}$, $N_0 = 10^{17}\ \text{cm}^{-3}$, and $d = 0.6$.

The following are the relationships between diffusion coefficient and electric mobility:

(i) Einstein's relations are

$$\begin{aligned} D_n &= \frac{kT}{q}\mu_n, \\ D_p &= \frac{kT}{q}\mu_p. \end{aligned} \tag{25}$$

(ii) The Shockley-Read-Hall lifetime recombination is

$$\tau_{\text{SRH}} = \frac{\tau_0}{1 + (N/K)}, \quad K = 7 \times 10^{15}\ \text{cm}^{-3} \tag{26}$$

(iii) The lifetime of radiation recombination is

$$\tau_{rad} = \frac{1}{BN}, \quad B = 2 \times 10^{-14}\ \text{cm}^3/\text{s} \tag{27}$$

(iv) The Auger lifetime recombination is

$$\tau_{\text{Aug}} = \frac{1}{CN^2} \tag{28}$$

where silicon-n is $C_n = 10^{-31}\ \text{cm}^6/\text{s}$ and silicon-p is $C_p = 2.8 \times 10^{-31}\ \text{cm}^6/\text{s}$

(v) Total lifetime is

$$\frac{1}{\tau} = \frac{1}{\tau_{\text{SRH}}} + \frac{1}{\tau_{\text{rad}}} + \frac{1}{\tau_{\text{Aug}}} \tag{29}$$

(vi) The lengths of the diffusion of minority carriers are

$$\begin{aligned} \text{Electrons}: \ L_n &= \left(D_n \tau_n\right)^{1/2} \\ \text{Holes}: \ L_p &= \left(D_p \tau_p\right)^{1/2} \end{aligned} \tag{30}$$

(vii) The variation in bandwidth forbidden at high doping levels is

$$\Delta E_G = a\left[\left(\frac{N^*}{N}\right)^b + 1\right]^{-c} \tag{31}$$

where $a = 0.231$ eV; $b = 3/4$; $c = 2/3$; and $N^* = 10^{20}\ \text{cm}^{-3}$

(viii) The effective intrinsic concentration of carriers at high levels of doping is

$$n_{i,ef}^2 = n_i^2 \ \exp\ \frac{\Delta E_G}{kT} \tag{32}$$

(ix) The effective recombination speed at the P^+P interface of the emitter is

$$s_{p,ef} = \frac{D_P^+}{L_p^+}\frac{n_{i+}^2}{n_i^2}\frac{N_D}{N_D^+}\frac{\left(s_P^+ L_p^+/D_p^+\right) + th\left(w_B^+/L_p^+\right)}{1 + \left(s_p^+ L_p^+/D_p^+\right) th\left(w_B^+/L_p^+\right)} \tag{33}$$

(x) The density of saturation power at the P^+P emitter is

$$J_{b0}^+ = \frac{qD_p {n_i}^2}{L_p N_D}\frac{\left(s_{p,ef} L_p/D_p\right) + th\left(w_B/L_p\right)}{1 + \left(s_{p,ef} L_p/D_p\right) th\left(w_B/L_p\right)} \tag{34}$$

(xi) The effective recombination speed on the interface on the base N^+N is

$$s_{n,ef} = \frac{D_n^+}{L_n^+}\frac{n_{i+}^2}{n_i^2}\frac{N_A}{N_A^+}\frac{(s_n^+ L_n^+/D_n^+) + th(w_B^+/L_n^+)}{1 + (s_n^+ L_n^+/D_n^+) th(w_B^+/L_n^+)} \tag{35}$$

(xii) The density of saturation power on the base N^+N is

$$J_{b0}^+ = \frac{qD_n {n_i}^2}{L_n N_A}\frac{\left(s_{n,ef} L_n/D_n\right) + th(w_B/L_n)}{1 + \left(s_{n,ef} L_n/D_n\right) th(w_B/L_n)} \tag{36}$$

(xiii) Total saturation power is

$$\begin{aligned} I_0 &= J_{e0} A_E + J_{b0} A_{B,\text{pas}} + J_{b0}^+ A_{B,\text{met}} \\ A_{B,\text{pas}} + A_{B,\text{met}} &= A_{\text{cel}} \\ J_0 &= \frac{I_0}{A_{\text{cel}}} \end{aligned} \tag{37}$$

(xiv) The open circuit voltage is

$$V_{OC} = \frac{kT}{q} \cdot \ln\left(\frac{J_{SC}}{J_0}\right) \tag{38}$$

(xv) The efficient conversion of solar energy is

$$\eta = \frac{J_{SC} \cdot V_{OC} \cdot f}{P_{\text{solar}\,a}} \tag{39}$$

(xvi) The solar power in conditions AM 1.5 is

$$P_{\text{solar}\,a} = 100\ \text{mW/cm}^2 \tag{40}$$

(xvii) The average short-circuit current density value for an AM spectrum 1.5 is

$$J_{SC} = 35\ \text{mA/cm}^2 \tag{41}$$

3.1. The Effective Recombination Velocities from an Emitter's Interface P^+/P Dependent on Recombination Velocities on the Region's P^+ Surface of Emitter $s_n{}^+$. From Figures 10–12, we observe that if at the emitter's surface, the recombination velocity is 10^5 cm/s for a doping concentration of the emitter of $10^{17}\ \text{cm}^{-3}$, the recombination velocities decrease to a value of $s_{n,ef} = 10^3$ cm/s, $s_{n,ef} = 10^2$ cm/s, and $s_{n,ef} = 1$ cm/s, if an additional diffusion P^+ is used with a concentration of $10^{17}\ \text{cm}^{-3}$, $10^{18}\ \text{cm}^{-3}$, and $10^{19}\ \text{cm}^{-3}$, respectively. The minimal value for the effective recombination velocities on the interface P^+/P of emitter $s_{n,ef}$ is obtained in the case of $N_A{}^+ = 10^{18}\ \text{cm}^{-3}$, $w_E{}^+ = 0.5 \times 10^{-4}$ cm, and $\tau_{\text{SRH}} = 5\ \mu$s (see Figure 11), while using a doping concentration of the emitter of $N_A{}^+ = 10^{15}\ \text{cm}^{-3}$, and its value becomes 0.2777 cm/s.

3.2. The Effective Recombination Velocities from Base's Interface $N/N^+ s_{p,ef}$ Dependent on Base's Strongly Doped Concentration $N_D{}^+$. A similar effect to the one of the effective recombination velocities from interface P^+P is obtained at the contact surface of Al base where the recombination velocity is 10^6 cm/s (see Figures 13–14). If on the back of the wafer an additional layer of diffusion N^+ is made with a thickness of 5 μm (see Figure 13) and a concentration of $10^{19}\ \text{cm}^{-3}$, then the effective recombination velocities go down to the value of 10 cm/s for a base doped to $10^{15}\ \text{cm}^{-3}$. The minimal value for the effective recombination value from base's interface $N/N^+ s_{p,ef}$ is obtained in the case of $w_B{}^+ = 20$

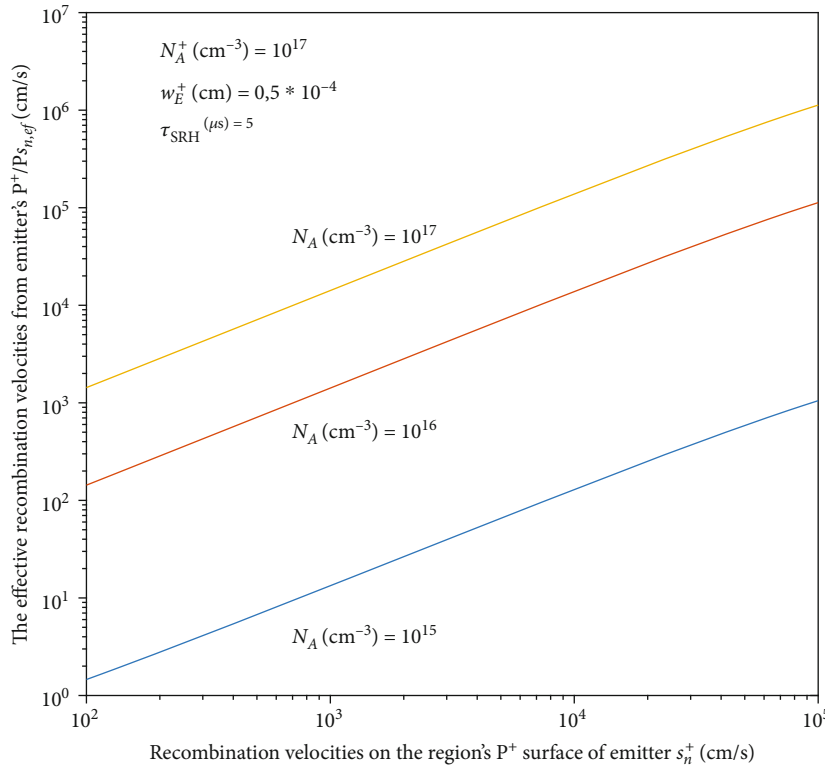

Figure 10: The effective recombination velocities from the emitter's interface P$^+$/P $s_{n,ef}$ are dependent on recombination velocities on the region's P$^+$ surface of emitter $s_n{}^+$ in the following conditions: $N_A{}^+ = 10^{17}$ cm^{-3}, $w_E{}^+ = 0.5 \times 10^{-4}$ cm, and $\tau_{SRH} = 5\,\mu$s.

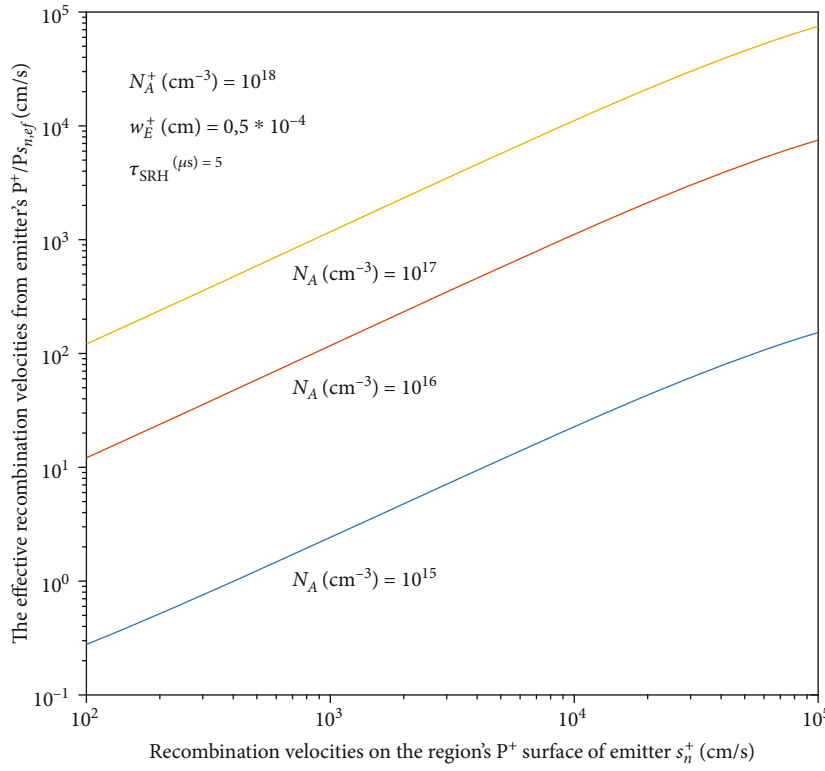

Figure 11: The effective recombination velocities from the emitter's interface P$^+$/P $s_{n,ef}$ are dependent on recombination velocities on the region's P$^+$ surface of emitter $s_n{}^+$ in the following conditions: $N_A{}^+ = 10^{18}$ cm^{-3}, $w_E{}^+ = 0.5 \times 10^{-4}$ cm, and $\tau_{SRH} = 5\,\mu$s.

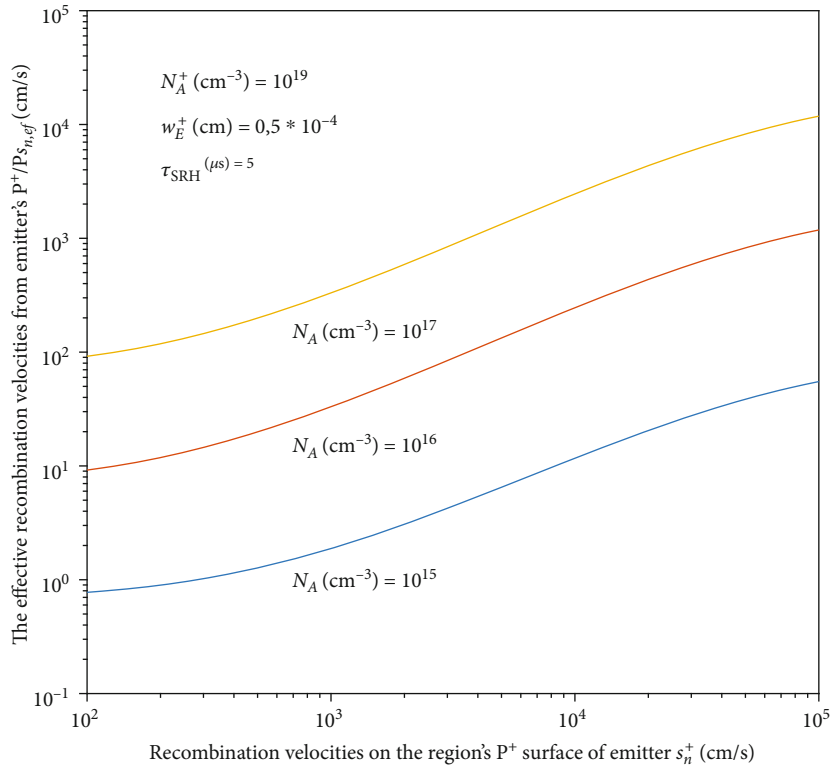

Figure 12: The effective recombination velocities from the emitter's interface P^+/P $s_{n,ef}$ are dependent on recombination velocities on the region's P^+ surface of emitter $s_n{}^+$ in the following conditions: $N_A{}^+ = 10^{19}$ cm^{-3}, $w_E{}^+ = 0.5 \times 10^{-4}$ cm, and $\tau_{SRH} = 5\,\mu$s.

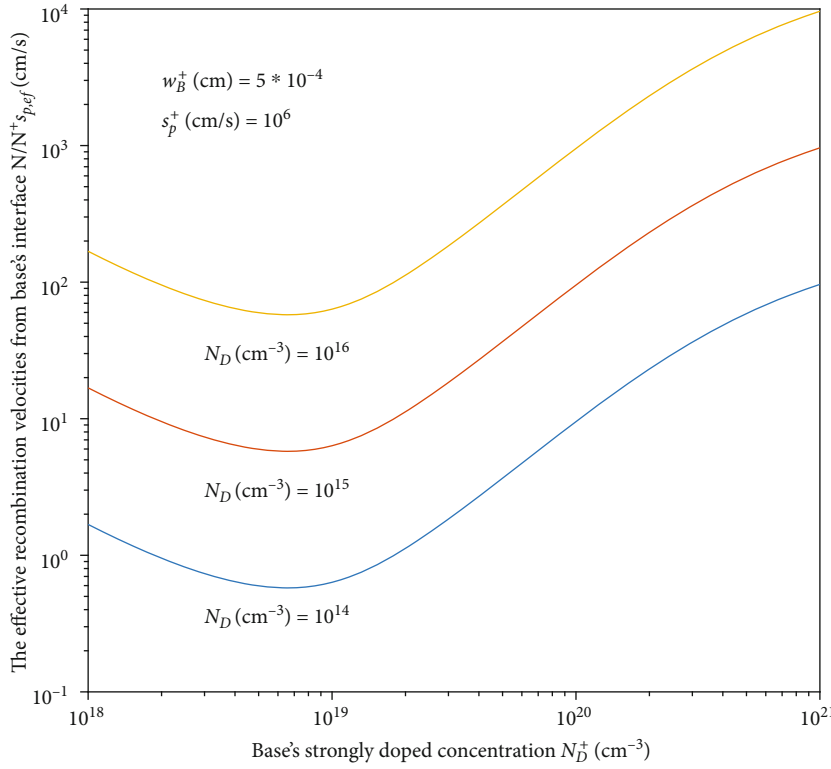

Figure 13: The effective recombination velocities from base's interface $N/N^+s_{p,ef}$ dependent on base's strongly doped concentration $N_D{}^+$ in the case of $w_B{}^+ = 5 \times 10^{-4}$ cm and $s_p{}^+ = 10^6$ cm/s.

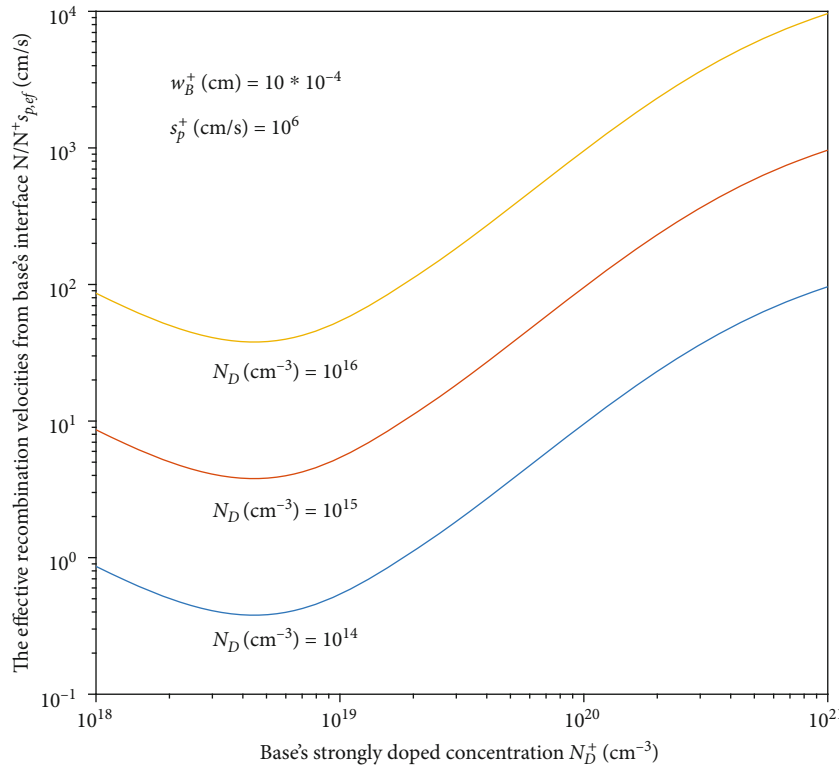

FIGURE 14: The effective recombination velocities from base's interface N/N$^+s_{p,ef}$ dependent on base's strongly doped concentration $N_D{}^+$ in the case of $w_B{}^+ = 10 \times 10^{-4}$ cm and $s_p{}^+ = 10^6$ cm/s.

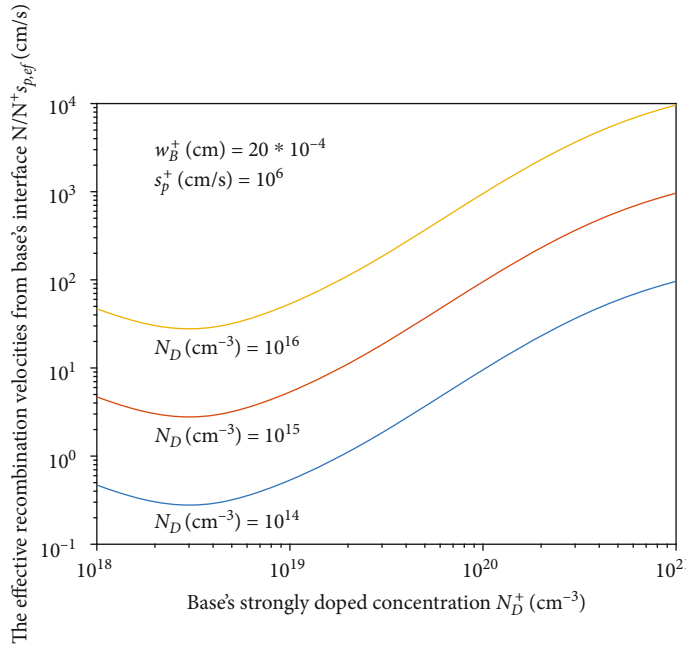

FIGURE 15: The effective recombination velocities from base's interface N/N$^+s_{p,ef}$ dependent on base's strongly doped concentration $N_D{}^+$ in the case of $w_B{}^+ = 20 \times 10^{-4}$ cm and $s_p{}^+ = 10^6$ cm/s.

$\times 10^{-4}$ cm and $s_p{}^+ = 10^6$ cm/s (see Figure 15), using a doping concentration of $N_D = 10^{14}$ cm^{-3}, this value being of 0.5 cm/s.

The obtained values are available because they accomplish the following technological conditions:

(i) The average value of phosphorus base doping: $N_D = 1.5 \bullet 10^{14}$ cm^{-3}

(ii) The average value of emitter layer diffusion: $N_A = 10^{17}$ cm^{-3}

(iii) The depth of junction p-n emitter-base: $w_E = 5\,\mu$m

4. Conclusions

In this study, current-voltage characteristics of a photovoltaic solar cell, measured in various conditions of illumination and temperature, are presented. Also, based on the analysis of these characteristics, the technological characteristics of the studied solar cell are determined.

A mathematical model of the physical processes which leads to the generation of electric currents in a complex photovoltaic solar cell type P^+PNN^+ with a finite recombination velocity on the surface is proposed.

Both recombination velocities of charge carriers on the surface and regions N^+N and P^+P are essential in photovoltaic solar cell type P^+PNN^+ functioning. In a photovoltaic solar cell with a p-n junction, the saturation current is given by the recombination on the two faces of the wafer.

The analysed case was accomplished for $\tau_{SRH} = 5\,\mu$s for the purpose of the correlation of the experimental data with theoretical models using Matlab.

The initial wafers of silicon are not competitive, but the application of the diffusion process of metallic contamination impurities by doping a phosphorus layer on the back of wafers led to a significant improvement of the lifetime in their volume.

Data Availability

The data used to support the findings of this study are available from the corresponding author upon request.

Conflicts of Interest

The authors declare that they have no conflicts of interest.

Acknowledgments

The authors would like to thank Dan Sachelarie for his helpful discussion and ICPE Bucharest for measurements of SEM and X-ray diffraction.

References

[1] R. P. Smith, A. A.-C. Hwang, T. Beetz, and E. Helgren, "Introduction to semiconductor processing: fabrication and characterization of *p-n* junction silicon solar cells," *American Journal of Physics*, vol. 86, no. 10, pp. 740–746, 2018.

[2] A. E. Becquerel, "Recherches sur les effets de la radiation chimique de la lumière solaire au moyen des courants électriques," *Comptes rendus de l'Académie des Sciences*, vol. 9, pp. 145–149, 1839.

[3] W. G. Adams and R. E. Day, "V. The action of light on selenium," *Proceedings of the Royal Society of London*, vol. 25, no. 171-178, pp. 113–117, 1877.

[4] C. Yu, S. Xu, J. Yao, and S. Han, "Recent advances in and new perspectives on crystalline silicon solar cells with carrier-selective passivation contacts," *Crystals*, vol. 8, no. 11, p. 430, 2018.

[5] K. Yamamoto, K. Yoshikawa, H. Uzu, and D. Adachi, "High-efficiency heterojunction crystalline Si solar cells," *Japanese Journal of Applied Physics*, vol. 57, no. 8S3, article 08RB20, 2018.

[6] J. Haschke, O. Dupré, M. Boccard, and C. Ballif, "Silicon heterojunction solar cells: Recent technological development and practical aspects - from lab to industry," *Solar Energy Materials and Solar Cells*, vol. 187, pp. 140–153, 2018.

[7] W.-J. Ho, J.-J. Liu, Y.-C. Yang, and C.-H. Ho, "Enhancing output power of textured silicon solar cells by embedding indium plasmonic nanoparticles in layers within antireflective coating," *Nanomaterials*, vol. 8, no. 12, p. 1003, 2018.

[8] M. Müller, G. Fischer, B. Bitnar et al., "Loss analysis of 22% efficient industrial PERC solar cells," *Energy Procedia*, vol. 124, pp. 131–137, 2017.

[9] C.-L. Cheng, C.-C. Liu, and C.-T. Yeh, "Photovoltaic and physical characteristics of screen-printed monocrystalline silicon solar cells with laser doping and electroplated copper," *International Journal of Photoenergy*, vol. 2019, Article ID 5372904, 9 pages, 2019.

[10] S. Chander, A. Purohit, A. Sharma, Arvind, S. P. Nehra, and M. S. Dhaka, "A study on photovoltaic parameters of monocrystalline silicon solar cell with cell temperature," *Energy Reports*, vol. 1, pp. 104–109, 2015.

[11] E. Cuce, P. M. Cuce, and T. Bali, "An experimental analysis of illumination intensity and temperature dependency of photovoltaic cell parameters," *Applied Energy*, vol. 111, pp. 374–382, 2013.

[12] A. K. Biswas, S. Biswas, and A. Sinha, "The photocurrent and spectral response of proposed P^+PNN^+ silicon solar cells," *International Journal of Renewable Energy Research*, vol. 8, no. 1, pp. 82–89, 2018.

[13] H. Sun, J. Wei, Y. Jia, X. Cui, K. Wang, and D. Wu, "Flexible carbon nanotube/mono-crystalline Si thin-film solar cells," *Nanoscale Research Letters*, vol. 9, no. 1, p. 514, 2014.

[14] T. Saga, "Advances in crystalline silicon solar cell technology for industrial mass production," *NPG Asia Materials*, vol. 2, no. 3, pp. 96–102, 2010.

[15] A. M. Bagher, M. M. A. Vahid, and M. Mohsen, "Types of solar cells and application," *American Journal of Optics and Photonics*, vol. 3, no. 5, p. 94, 2015.

[16] A. Goodrich, P. Hacke, Q. Wang et al., "A wafer-based monocrystalline silicon photovoltaics road map: utilizing known technology improvement opportunities for further reductions in manufacturing costs," *Solar Energy Materials and Solar Cells*, vol. 114, pp. 110–135, 2013.

[17] C. P. Fluieraru, *Studies and research on the using monocrystalline silicon solar cells manufacturing, [Ph.D. thesis]*, Valahia Univeristy Press, Târgoviște, Romania, 2013.

[18] A. M. Green, *Third Generation Photovoltaics, Advanced Solar Energy Conversion*, Springer, 2003.

[19] H. Andrei, T. Ivanovici, G. Predușcă, E. Diaconu, and P. C. Andrei, "Curve fitting method for modeling and analysis of photovoltaic cells characteristics," in *Proceedings of 2012 IEEE International Conference on Automation, Quality and Testing, Robotics*, pp. 307–312, Cluj-Napoca, Romania, 2012.

[20] N. Jenny, *The Physics of Solar Cells*, Imperial College Press, 2003.

[21] W. Shockley and H. J. Queisser, "Detailed Balance Limit of Efficiency of *p-n* Junction Solar Cells," *Journal of Applied Physics*, vol. 32, no. 3, pp. 510–519, 1961.

[22] A. S. Brown and M. A. Green, "Limiting efficiency for current-constrained two-terminal tandem cell stacks," *Progress in Photovoltaics: Research and Applications*, vol. 10, no. 5, pp. 299–307, 2002.

[23] E. V. Stoian, C. P. Fluieraru, and M. C. Enescu, "Determining electromagnetic attenuation for material composites polymer," *Scientific Bulletin of the Electrical Engineering Faculty*, vol. 12, no. 3, pp. 49–53, 2012.

[24] C. Z. Rizescu, E. V. Stoian, D. N. Ungureanu, Z. Bacinshi, and F. C. Petre, "Study on powdered samples and particle size determinations by scanning electronic microscopy (SEM), diffraction of X-rays," *International Journal of Mechanics*, vol. 5, no. 3, pp. 138–147, 2011.

[25] D. K. Schroder, *Semiconductor Material and Device Characterization*, John Willey & Sons Inc., 3rd edition, 2006.

[26] P. A. Cotfas and D. T. Cotfas, "Design and implementation of RELab system to study the solar and wind energy," *Measurement*, vol. 93, pp. 94–101, 2016.

[27] D. T. Cotfas, P. A. Cotfas, and O. M. Machidon, "Study of temperature coefficients for parameters of photovoltaic cells," *International Journal of Photoenergy*, vol. 2018, Article ID 5945602, 12 pages, 2018.

[28] D. Sachelarie, *Semiconductoare si Heterostructuri*, Matrix Rom, 2000.

[29] D. Sachelarie, *Bazele Dispozitivelor Semiconductoare*, Matrix Rom, 2003.

[30] D. Sachelarie, G. Predușcă, and H. G. Coandă, *Probleme Fundamentale de Microelectronică*, MatrixRom, București, Romania, 2004.

[31] G. Predușcă and D. Sachelarie, *Matlab Pentru Microelectronică*, MatrixRom, București, Romania, 2011.